Astron. Astrophys. 296, 359–369 (1995)

ASTRONOMY AND ASTROPHYSICS

Dynamics of the Abell 98 cluster and the radio structure of 4C+20.04

J. Krempeć-Krygier[1], **and B. Krygier**[2]

[1] N. Copernicus Astronomical Center, Astrophysical Lab., Toruń, Poland
[2] Toruń Radio Astronomy Observatory, Toruń, Poland

Received date 27 January 1994 / Accepted 25 September 1994

Abstract. The dynamics of the Abell cluster 98 (A 98) and its two subclusters, A 98S and A 98N, distinguished in the galaxy and the X-ray surface brightness distributions, have been discussed. A 98S and A 98N, separated by 8.93 arcmin, are moving with the relative radial velocity of 455 [km s^{-1}] and are being merged. We have used the radial and the circular orbit models for two point masses of A 98S and A 98N estimated from the virial theorem and have derived the inclination angles of the orbital planes to the plane of sky. In the projection on the sky A 98S and A 98N lay at the position angle of 351 deg, measured from the N– toward the E-S-W – direction, which is close to those of the optical major axis and of radio structure of radio galaxy 4C+20.04A (0043+2011A). The comparison of the thermal intracluster/intergalactic (ICM/IGM) gas pressure with the nonthermal (minimum) one indicates that radio lobes are confined by thermal pressure. However, the structure of radio jets is influenced by the hot (ICM/IGM) gas disturbed by the merger of subclusters.

Key words: clusters of galaxies: A 98 – galaxies: jets – radio continuum: galaxies – galaxies: 4C+20.04A

1. Introduction

In recent years both the X-ray and the optical surveys have revealed a significant level of substructure in both the gaseous (ICM) and the galaxy component of clusters of galaxies (Rhee et al. 1991; Forman & Jones 1982; Beers et al. 1991; Sarazin et al. 1992). The degree of subclustering in clusters of galaxies yields the direct information on their dynamical state. If clusters are relaxed, then subclusters should not be present. On the other hand, if relaxation has not occurred, then clusters are dynamically young objects and subclusters should be common. The optical counts of number of galaxies reveal that approximately 40 % of clusters show some type of substructure (Geller & Beers 1982), while the numerical simulation of the evolution of galaxy clusters indicates that at least 50 % of apparently relaxed clusters contain significant substructures (Salvador-Solé et al. 1993). One possible explanation for the origin of observed substructure is subcluster mergers (Mc Glynn & Fabian 1984). Malumuth (1992) suggested that even the clusters of galaxies containing the bright cD galaxies with large peculiar velocities, such as A1146, A1795, A2029, A2634 and A2670, can be formed by mergers in a virialized cluster.

In the present paper, we will discuss the Abell cluster, A 98, which reveals the subclusters in the velocity (Sect. 2) as well as in the galaxy and the gaseous components (Sect. 3). We assume the Hubble constant $H_o = 50$ [km (s Mpc)$^{-1}$] and $q_o = 0.5$ throughout this paper. Then, at a distance of A 98 (z = 0.1047), 1 arcsec corresponds to 2.5646 h^{-1} kpc (where $H_o = 50\,h$[km (s Mpc)$^{-1}$]).

2. Dynamics of A 98

A 98 is rich (R=3), quite distant (D=5) cluster of galaxies (Abell et al. 1989) without the large cD galaxy at its center (the Bautz-Morgan type - BM:II-III). It contains 185 galaxies within a magnitude range m_3 to m_3+2 designated as N_c in next Section (where m_3 is the magnitude of the third bright cluster member) and the red magnitude of its tenth bright cluster member is 16.9 mag.. The X-ray data of A 98 (Forman et al. 1981; Henry et al. 1981) and the galaxy distribution (Dressler 1978a, 1978b) indicate that A 98 consists of two subclusters (subclumps), namely the south (A 98S) and the north (A 98N) ones. In projection on the sky A 98S (z=0.1054) has a center close to the position of radio galaxy 4C+20.04A (0043+2011A, z=0.1034), while the center of A 98N (z=0.1037) coincides with the position of the galaxy 0043+2020 (z=0.1028). They are separated by 8.93arcmin (1.374Mpc).

The radial velocities for galaxies in A 98 were discussed by Faber & Dressler (1977), Dressler (1978), Beers et al.(1982) and Zabludoff et al (1990). We compiled all the observed line-of-sight heliocentric velocities of galaxies in A 98, divided them into two subclusters, A 98S and A 98N, and considered the dy-

Send offprint requests to: J. Krempeć-Krygier

namics of a whole cluster and of both subclusters separately. If one adopts, according to the Abell definition of the cluster radius, 3Mpc as a radius of A 98, then its angular radius will be 19.5 $h$arcmin. We have assumed the angular radii of subclusters as traced by the observed galaxy distributions given by Zabludoff et al. (1990). They are consistent with those estimated by Dressler (1978b) and are given in the Table 1 as R_A. The derived comoving luminosity distances DIS are also inserted in Table 1. We derived the relativistic line-of-sight velocities of galaxies, the mean relativistically corrected cluster radial velocities – V_{rcl} and the dispersion of radial velocities σ according to formulae given by Danese et al. (1980). As is seen from the Table 1, two subclusters of A 98, i.e. A 98S and A 98N, are well separated in radial velocities by V_{rel} = 455[km s^{-1}]. We assumed, usually adopted, the null hypothesis that the radial velocity distributions are the Gaussians. However, the recent measurements of radial velocities of clusters and groups of galaxies indicate that only few of them have achieved dynamical equilibrium, when the Gaussian distributions of radial velocity might be expected. Thereafter, we compare the histograms of observed radial velocities for galaxies in A 98 with the calculated Gaussian ones in Fig.1. The bins of radial velocities are 400[km s^{-1}] wide.

We used the χ^2 test to analyse the deviations (see Table 1). Besides, we derived the higher order moments of the normal distribution, namely the third order momentum – the skewness S and the fourth order momentum – the excess (also called the kurtosis) E. As is seen from Table 1 the skewness is insignificant, while the excess being statistically significant is largest for A 98S. Generally, there is a deficit of observed number of galaxies in velocity bins relative to the Gaussian ones. We also applied other known tests of non – normality, i.e. the a – and the u – tests described by Yahil & Vidal (1977) as well as the classic biweight locations (Beers et al. 1990) – the sample median MED and an auxiliary estimate of scale – the median absolute deviation from the sample median – MAD (see Table 1). Basing upon all the above mentioned tests and parameters it is worth noting that the most disturbed distribution of radial velocities for galaxies and the largest deviation from the Gaussian occur in A 98S, while the smallest ones in A 98N. However, the number of discussed galaxies is small (N in Table 1) and the further analysis based upon a larger amount of the data is necessary.

Schindler & Böhringer (1993) presented the N-body simulations of the evolution of galaxy clusters. They considered a cluster collapse, a collision of subclusters and a steady infall of galaxies into a cluster. They also presented the velocity distributions at different times in their collision model, in which two already virialised small clusters collide to form a large cluster of galaxies. We compare the observed distributions of radial velocities of galaxies in A 98S and A 98N in Fig.2. The ratio of virial masses of A 98S and A 98N within their cores is about 2.9. Their maxima of velocity distributions are removed by about 200[km s^{-1}] and the velocity distribution of galaxies in A 98S is slightly asymmetric.

Accordingly, the subclusters start to merge since they are distant in projection on the sky and might be little accelerated having slightly different velocity distributions. However, it is

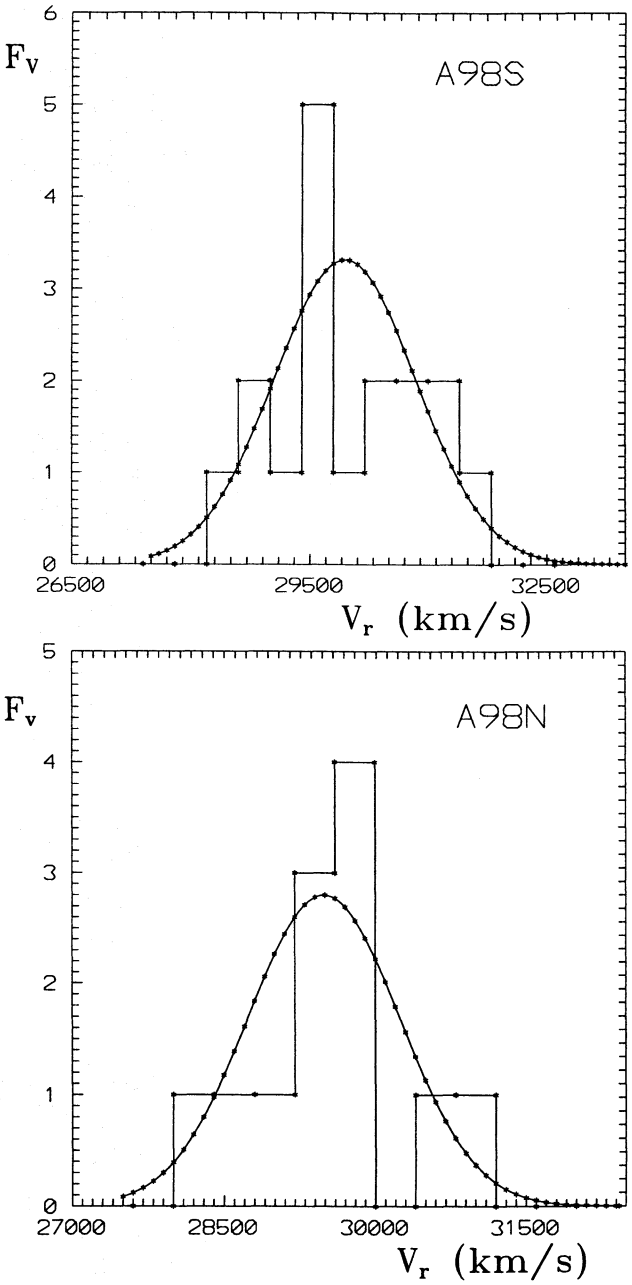

Fig. 1. Comparison of the radial velocity distributions for galaxies in the bins of 400 [kms^{-1}] with the Gaussian ones for A 98S and A 98N

extremely difficult to determine the degree of virialisation of a cluster and to decide if subclumps/ subclusters are being collapsed or merged for such a limited number of velocity data as in the case of A 98. According to Henriksen (1993) during the premerger stage in hierarchical clustering, there are two galactic and two gas components and no cooling flows. Such stage of subcluster evolution occurs in A 98. On the other hand, the recent discussion of the X-ray and of the galaxy spatial distributions by Davis & Mushotzky (1993) has confirmed the existence of the X-ray substructures even in such regular clusters as A1656 (Coma) and A2256 and the recent ROSAT observa-

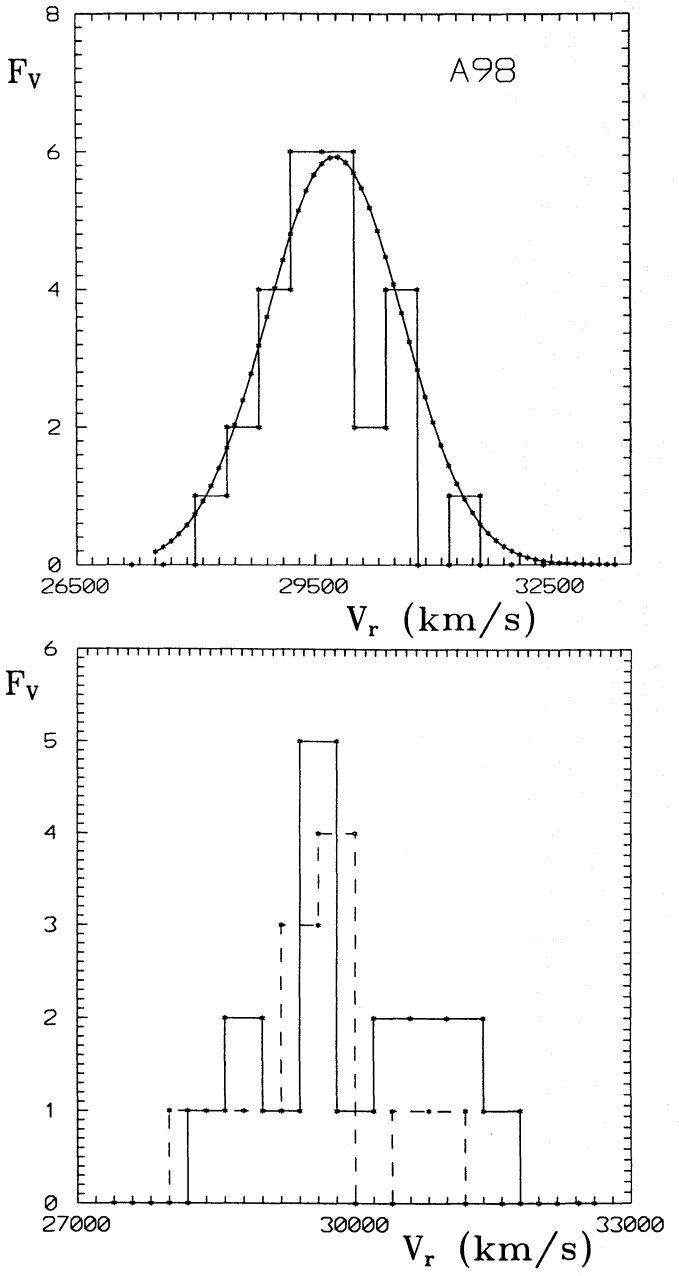

Fig. 2. The same as Fig.1 for A 98 and the histograms of the observed radial velocities for galaxies in A 98S (solid line) and A 98N (dashed line)

Table 1. Dynamical data for A 98

	A 98S	A 98N	A 98
N	17	12	29
z	0.1054	0.1037	0.1047
R_A[arcmin]	11.04	5.40	13.73
R_A[Mpc]	1.70	0.82	2.11
DIS[Mpc]	586.13	577.37	582.50
V_{rcl} [km s^{-1}]	29945	29490	29757
σ	901	751	859
S	0.11	0.03	0.21
E	-1.21	-0.63	-0.75
χ^2/dof	6.8788/10	5.0518/10	5.1282/10
P(%)	74.2	88.6	87.9
a	0.839	0.753	0.793
u	3.866	4.0655	5.012
MED [km s^{-1}]	29734	29496	29701
MAD	720	325	687

tions show that the collision of subclusters is a frequent process (Schwarz et al. 1992; Briel et al. 1992). If A 98S and A 98N are being merged, one may adopt two body dynamical model for A 98. We applied two dynamical models, namely the radial orbit model of Beers et al. (1982) and the circular orbit model of Fitchett et al. (1987). Unfortunately, we do not know the true velocity difference V and the true separation R of two subclusters. We measure only the projected values, V_{rel} and R_p. In the radial orbit model one has: $V_{rel} = V \sin\alpha$ and $R_p = R\cos\alpha$, where α is a projection angle with respect to a plane of the sky and $V_{rel} = V_{rcl}$(A 98S) – V_{rcl}(A 98N). Knowing the total mass of a cluster and the projected separation of subclusters one may derive a relation between V_{rel} and α according to formula given by Beers et al. (1991), i.e. $V_{rel} = \sqrt{(\frac{2\,G\,M_{tot}}{R_p})}\sin\alpha\sqrt{(\cos\alpha)}$, where G is the gravitational constant and M_{tot} – the total mass of a cluster. The calculated relations are shown in Fig.3. Since we have applied the virial theorem for mass estimation, we have assumed that each of the subclusters is bound and near equilibrium and that the galaxy orbits are random. The first of these assumptions is probably valid. On the other hand, a cluster as a whole may not be relaxed. A 98 is a bound system and the subclusters are in bound - ingoing regime with a 94 % probability (Beers et al. 1982). Then, our value of V_{rel}, i.e. 455[km s^{-1}], leads to α equal to about 23 and 15.6 deg for $M_{tot} = 2.35 \cdot 10^{14}$ and $4.75 \cdot 10^{14}\,M_\odot$ respectively. The small value of α indicates that the subclusters move in the plane close to the plane of the sky and their projection distance differs only slightly from the true one.

In the circular orbit model, the subclusters are falling into the center of cluster having some orbital angular momentum. Then, in a spherical polar system with angle θ measured from the normal to the orbital plane and the angle Φ measured from the line joining the two subclusters, the $V_{rel}(\theta)$ relation is: $V_{rel} = V_{sys}\sqrt{(\lambda)}\sqrt{(\lambda^2 - \cos^2(\theta))}$, where λ is a ratio of projected separation of subclusters to true one, i.e. $\lambda = \frac{R_p}{R}$, V_{sys} being the circular orbit velocity (V_{circ}) is given by $V_{sys} = \sqrt{(\frac{G\,M_{tot}}{R_p})}$ and θ is contained within a range: $\arccos\lambda \leqq \theta \leq \pi - \arccos\lambda$. We derived $V_{rel}(\theta)$ relations for different values of λ, namely λ equal to 0.3, 0.5, 0.6, 0.7, 0.9 and 1.0 (see Fig.4). It is seen in Fig.4, that for A 98 having $V_{rel} = 455$[km s^{-1}], the values of λ smaller than 0.7 are inappriopriate for the most probable mass of A 98, i.e. $M_{tot} = 4.75 \cdot 10^{14} M_\odot$, what gives an upper limit on θ. It is worth noting that the circular or-

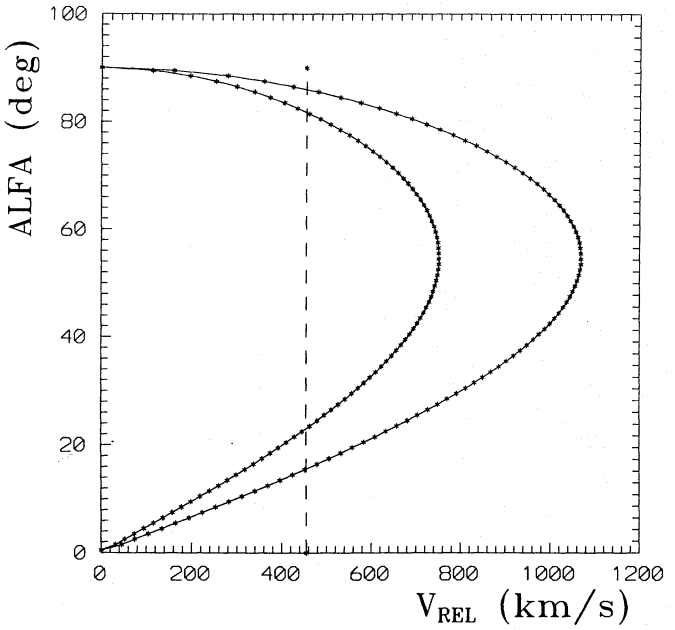

Fig. 3. Plot of the projection angle on the plane of the sky α versus the velocity difference V_{rel} for a radial orbit model for two values of the total system mass M_{tot}, i.e. $2.35 \cdot 10^{14}\, M_{\odot}$ (inner curve) and $4.75 \cdot 10^{14}\, M_{\odot}$ (outer curve). The vertical dashed line indicates the observed relative cluster velocity

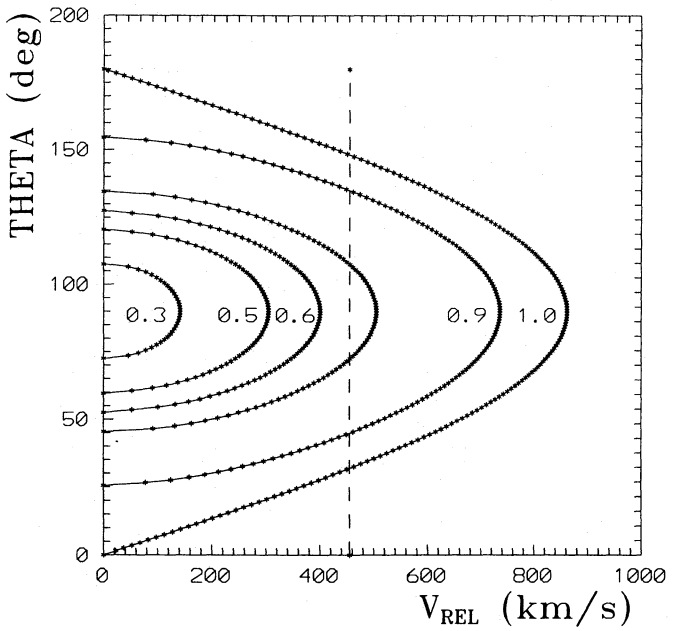

Fig. 4. Relations between the angle normal to the orbital plane θ and the velocity difference V_{rel} for the circular orbit model derived for different values of λ, namely 0.3, 0.5, 0.6, 0.7, 0.9, 1.0 (see designation), and $M_{tot} = 4.75 \cdot 10^{14}\, M_{\odot}$. The vertical dashed line indicates the observed relative cluster velocity

bit model does not determine the system parameters uniquely. Nevertheless, it gives more reasonable projection angles. For A 98 having $M_{tot} = 4.75 \cdot 10^{14} M_{\odot}$, $V_{circ} = 862[\mathrm{km\,s^{-1}}]$ and $V_{rel} = 455[\mathrm{km\,s^{-1}}]$ the derived parameters are, as follows:
$\lambda = 0.7$; $\theta = 72.3$ deg; $R = 1.96$ Mpc
$\lambda = 0.9$; $\theta = 44.8$ deg; $R = 1.53$ Mpc
$\lambda = 1.0$; $\theta = 31.9$ deg; $R = 1.37$ Mpc
Unfortunately, the values of θ depend upon M_{tot}, which is not accurately known.

In their recent discussion of the mass function of clusters of galaxies, Bahcall & Cen (1993) analyse the different methods of estimation of an average mass of a typical rich cluster. Firstly, one can approximate an average mass of a typical rich cluster as $M(\leqq 1.5\, h^{-1}\mathrm{Mpc}) = 0.6 \cdot 10^{13\pm0.12}\, N_c\, h^{-1} M_{\odot}$. Putting for A 98, N_c=185 and h = 0.5 we derived quite large mass equal to $2.22 \cdot 10^{15} M_{\odot}$. Secondly, using for a cluster with an isothermal mass distribution the relation, $M(\leqq 1.5\, h^{-1}\mathrm{Mpc}) = 0.68 \cdot 10^{13} (\frac{\sigma}{100})^2$ (see Peebles 1992), we calculated the virial masses equal to $5.52 \cdot 10^{14}$, $3.83 \cdot 10^{14}$ and $5.02 \cdot 10^{14} M\odot$ for A 98S, A 98N and A 98 respectively. Besides, the relation of the cluster richness N_c with the radial velocity dispersion σ, i.e. $(\frac{\sigma}{100}) = (0.9 \pm 0.2)\sqrt{N_c}$, gives for derived values of σ, the number of galaxies equal to 100, 70 and 91 for A 98S, A 98N and A 98 respectively. Accordingly, we derived approximately the observed number of cluster galaxies summing the values calculated for subclusters. Hence, one may consider the subclusters A 98S and A 98N as virialised configuration with isothermal mass distribution. It is worth noting that cluster masses derived from above statistical relations are larger than the previous ones giving smaller projection angles.

On the other hand, the giant blue luminous arcs found in some distant and rich clusters of galaxies have been interpreted as gravitationally lensed images of background galaxies provided there is a significant amount of dark matter in these clusters (Tyson 1988; Tyson et al. 1990). Then, one can derive masses and the projected binding matter distribution of cluster of galaxies being the gravitational lenses by modelling of gravitational arcs (Blandford & Kochanek 1987; Bergmann et al. 1990). Accordingly, it is an independent measurement of cluster mass distribution. However, the modelling of gravitational lenses is concerned with the models of the surface density of continuous, smooth component representing the dark matter and clumpy components describing the luminous matter associated with individual galaxies. Therefore, an estimate of dark matter distribution in clusters of galaxies from arc models is rather questionable because we have many more free parameters than observational constraints. Only in cases, when we have a large number of multiple images, we can derive unequivocally the gravitational potential of the galaxy cluster (gravitational lens). Recently, it has been done by Mollier et al. (1993) for MS 2137–23 (z=0.313). They have derived that the core radius of the cluster is smaller than generally adopted and the amount of dark matter is large. However, using the Turner et al. criterion for the central surface density of gravitational lenses (Turner et al. 1984) we found that A 98S and A 98N would not be the gravitational lenses. Generally, the studies of the gravitational

Table 2. Physical parameters for A 98S and A 98N

Parameter	A 98S	A 98N
β_{imag}	0.67	1.03
β_{spec}		
for kT_x = 7keV	0.76	0.53
for kT_x = 3keV	1.78	1.24
For β_{spec}/7keV		
a_c(arcmin)	$3.4^{+0.7}_{-0.2}$	2.9
a_c(kpc)	526.093	442.683
n_o[cm^{-3}]	$1.67\,10^{-3}$	$2.31\,10^{-3}$
P_o	$1.87\,10^{-11}$	$2.59\,10^{-11}$
[dyn cm^{-2}]		
For β_{imag}		
a_c(arcmin)	3.0±0.3	6.4
R_x(arcmin)	9.91	7.91
n_o[cm^{-3}]	$1.99\,10^{-3}$	$7.04\,10^{-4}$
P_o	$2.24\,10^{-11}$	$7.90\,10^{-12}$
[dyn cm^{-2}]		
R_x(Mpc)	1.436	1.218
L_x	$6.40\,10^{43}$	$7.29\,10^{43}$
[erg s^{-1}]		
t_{ac}(yrs)	$2.23\,10^{9}$	$1.89\,10^{9}$

lens confirm the masses in rich clusters, which were implied by virial calculations.

The free fall times for subclusters are about a few times 10^8 up to $1.23\cdot10^9$yrs for q_o=0.5 and H_o = 50[km (s Mpc)$^{-1}$]. These time scales are of the same order as accustic ones, i.e. the time scale necessary for accustic waves to cross the cluster. On the other hand, the cooling time scales are longer than the Hubble time. Accordingly, A 98S and A 98N form a bound system and will merge in the free fall time scales.

3. Galaxy and the X-ray surface brightness distributions

The galaxy distribution function most commonly used to describe the virialised state is the King distribution (King 1966), i.e. $N(r) = N_o\,(1+(\frac{r}{r_c})^2)^{-1}$, where $N(r)$ is the projected surface density of galaxies, r is the projected radius, N_o – the central surface density and r_c – the core radius defined as a radius at which the projected density has dropped to half its central value. Dressler (1978a, 1978b) counted the galaxies in A 98 up to m_F = 19.2 mag. separately for two subclusters. He and later Henry et al. (1981) used these counts to derive the central densities N_o and the optical core radii r_c for A 98S and A 98N. Henry et al. (1981) derived the values, as follows: for A 98S – $r_c = 2.7 \pm 1.0$ arcmin, $N_o \simeq 2.0$ [gal. arcmin^{-2}]; for A 98N – $r_c = 3.0^{+4.0}_{-1.8}$ arcmin and $N_o \simeq 1.8$ [gal. arcmin^{-2}]. One usually takes the core radii to calculate the virial masses of clusters. Hence, we repeated the fitting to be awared of real uncertainties in the virial mass estimations. We derived the core radii equal to 2.0 and 1.0 arcmin as well as the central galaxy densities 3.1 and 4.6 [gal. arcmin^{-2}] for A 98S and A 98N respectively and for a whole cluster r_c = 2.6 arcmin and N_o = 2.3[gal. arcmin^{-2}]. These values are very uncertain, especially for subclusters, since one may hardly separate the members of each of them at greater distances from their centres. On the other hand, the fit is rather poor at large radii, where besides the tidal effects may be important. Hence, we consider our value of the core radius of A 98S as consistent with that one given by Henry et al. (1981), while the disagreement for A 98N is too large. However, the optical core radius of the order of 3 arcmin for A 98N seems to be overestimated. On the other hand, the r_c and N_o – values for a whole cluster are reasonable. We used the core radii and the radial velocity dispersions to calculate the central virial densities and masses by the relations: $\rho_{\rm vir} = \frac{9\sigma^2}{4\pi G r_c^2}$ and $M_{\rm vir} = \frac{4}{3}\pi r_c^3 \rho_{\rm vir}$. $M_{\rm vir}$ are the galaxy masses contained within the optical core radii of clusters and they were used in the dynamical considerations. Taking a radius of a cluster, which is 3 to 5 times larger than that of a core, one will calculate the smaller projection angles. However, a density decreases with radius and while the isothermal sphere approximation is reasonable for central region of a cluster, it fails for distant layers.

Forman et al. (1981) and Henry et al. (1981) presented the bimodal distribution of the X-ray surface brightness of A 98. The X-ray surface brigthness of A 98S is due only to the hot (ICM) gas, while that of A 98N contains also the contribution of central galaxy, i.e. 0043+2020, into the radiation of central region ($\lesssim$ 2arcmin). The azimuthally averaged surface brightness S(r) is fitted to the β model, as follows: $S(\mathrm{r}) = S_o\,(1+(\frac{r}{a_c})^2)^{-3\,\beta_{imag}+0.5}$. One has three fitting parameters, namely the X-ray central surface brightness S_o, the X-ray core radius a_c and β_{imag}. Henry et al. (1981) put β_{imag} = 1. We have taken their IPC counts of the Einstein satellite and used β_{imag} as a free parameter in the above relation. The values of the derived fitting parameters are given in Table 2.

We have not convolved the calculated surface brightness distributions with the IPC point-spread function, since derived a_c are much larger than the spatial resolution. On the other hand, the β parameter is a ratio of the kinetic energy of cluster galaxies to the thermal gas energy for the equilibrium configurations: $\beta_{spec} = \mu\, m_p \frac{\sigma^2}{k\,T_g}$, where μ is the mean molecular weight, m_p – the proton mass, k – the Boltzmann constant and T_g – the X-ray gas temperature. One usually assumes μ = 0.63 for solar element abundance. The X-ray gas temperature is calculated by fitting of the Raymond - Smith emissivity for the thermal bremsstrahlung and the line emission spectra to the X-ray spectral observations. Henry et al. (1981) used kT_x = 7 keV for both subclusters, while Ferretti et al. (1992) calculated kT_x = 3 keV for A 98S, then β(3keV) = $(\frac{7}{3})\beta$(7keV). The values of kT_x of 3 keV and of 7 keV correspond to $3.48 \cdot 10^7$ and $8.12 \cdot 10^7$K respectively. We derived for kT_x = 7 keV and our values of σ, the values of β_{spec} given in Table 2. Then, we put β_{spec} into the relation for the surface brightness distributions and obtained for the best fits the X-ray core radii and the central surface brightness given in Table 2. For kT_x = 3 keV we derived remarkably poorer fitting and we will not discuss it, although Feretti et al. (1992) assumed it for A 98S and derived β equal to 0.6, while

we derived β=1.78. There is no discrepency between β_{imag} and β_{spec} for A 98S for kT_x = 7 keV, while for A 98N it appears for kT_x = 7 keV. Besides, using the statistical relations between the observed cluster gas temperatures and cluster velocity dispersions given by White III (1991) and Lubin & Bahcall (1993) we derived for (A 98S) the values of kT_x of about 5.5 and 5.3keV respectively, while for (A 98N) – kT_x of about 3.9 keV. The calculated gas temperatures are consistent with those obtained from the observed relation given by Edge & Stewart (1991) for a sample of near clusters of galaxies, i.e. kT_x = 5.86keV for A 98S. Therefore, we consider kT_x(A 98S) = 3 keV as too low for the whole subcluster but it might refer to its central region as supported by a small value of a_c derived by Feretti et al. (1992). For A 98N the contribution of the central galaxy, i.e. 0043+2020, to the X-ray radiation within the central region was derived according to formula $S_x = A\,B\exp(-(\frac{r_x}{\delta})^2)$, where δ is the X-ray angular size of central galaxy. The fit of the observed and theoretical surface brightness distributions for A 98N is poorer and there is the " β – discrepancy " for kT_x = 7 keV.

Recently, Bahcall & Lubin (1994) have discussed the "β – discrepancy" problem. They have found that this discrepancy disappears for the assumed observed galaxy distributions in a cluster, i.e. $\rho(r) \sim r^{-2.4\pm0.2}$, instead of usually adopted steeper King law. However, it is worth noting that it is only the statistical approach. The recent ROSAT PSPC and HRI observations indicate that the "β – discrepancy" occurs for some clusters of galaxies (e.g. Henry et al. 1993). Then, it may result from the overestimation of the velocity dispersion due to the occurence of subclustering or from the underestimation of the gas temperature caused by small scale inhomogeneities (subclumps) of the ICM gas (Burns et al. 1994). Accordingly, the intrinsic physical properties of galaxy clusters can vary and contribute to the uncertainties in β. We believe that the ROSAT HRI observations and multifiber spectroscopy will lead for the better understanding and explanations of this discrepancy. It is specially desirable for A 98N, in which there is the central excess of the X – ray radiation due to the contribution of central galaxy, 0043+2020, or to cooling flow giving lower gas temperature at a center of the order of 3 or 4 keV and resolving "β – discrepancy".

For hydrostatic isothermal model (Cavaliere & Fusco-Femiano 1981) the X-ray radial surface brightness profile corresponds to the gas density and to the gas pressure profiles, as follows:

$$n(r) = n_o\,(1 + (\frac{r}{a_c})^2)^{-\frac{3}{2}\beta}$$

$$P(r) = P_o\,(1 + (\frac{r}{a_c})^2)^{-\frac{3}{2}\beta}$$

where n_o and P_o are the central electron (ion) density ($\rho_g = m_p \cdot n$, m_p – the proton mass) and the central gas pressure respectively. We derived central number densities from the X-ray luminosities of subclusters and used them to calculate the central gas pressures. The distributions of the thermal pressure of gas (P_g) will be compared with the nonthermal one (P_{min}) in next Section.

4. Radio sources in A 98

It is well known that radio galaxies in clusters of galaxies, particularly in rich ones, show often very complex morphology. The complex patterns seen in radio maps seem to be a result of processes in the nuclei of the galaxies together with interactions of radio emitting plasma with the (ICM) and the interstellar (ISM) medium. There are many general discussion of radio sources in the Abell clusters of galaxies (e.g. Ball et al. 1993; Burns 1990; Zhao et al. 1989). Nevertheless, it is not clear up to now how strongly radio phenomena are related to the environment. On the other hand, the merger of subclusters might produce the significant changes of the ICM, in which the multiple shocks and turbulence of different strengths depending upon the mass of subclumps would generate (Roettiger et al. 1993). Then, the different instabilities in the jets and the lobes will occur due to the motion of the ICM in respect to a galaxy.

The first ranked galaxy in A 98, namely 0043+2011A, is known as the F-R I radio galaxy 4C+20.04A (z=0.1034). Firstly it was considered as 4C+20.44. However, Slingo (1974) separated two radio sources A and B, only about 8 arcmin apart, i.e. the above mentioned radio galaxy designated also as A 98.1 and the radio galaxy 4C+20.04B (0044+2019=A 98.3, z=0.1044). 4C+20.04A is a double extended radio source, almost straight, although it is a prototype of the WATs (the WIDE ANGLE TAILED radio sources), with a prominent cluster galaxy laying between the two radio components. Sandage (1973) and Sandage & Hardy (1973) have measured the corrected brightness in different colors and the angular diameter of the first ranked galaxy in A 98 – the optical galaxy of 4C+20.04A, as follows: V = 15.55 mag, B = 16.51 mag and R = 14.68 mag and the diameter equal to 30.2 arcsec (76.648 kpc) for the isophote of 26 $mag\,(arcsec)^{-2}$. They have also estimated the corrected absolute visual magnitudes and the effective radii (the radii, which contain one-half of the light of the de Vaucouleurs law for projected density) of three bright galaxies in A 98, i.e. M_V equal to –22.43 mag, –21.68 mag and –21.06 mag for the first, second and third bright galaxy respectively. Abell et al. (1989) gave 13.43 arcsec (34.085 kpc) for a size of a major axis of this galaxy. On the other hand, Schneider et al. (1983) estimated the angular equivalent radii equal to 2.951 arcsec (7.490 kpc) and 2.884 arcsec (7.320 kpc) for the second and third bright galaxy compared to 5.495 arcsec (13.946 kpc) to the brightest one. Struble & Rood (1987) determined the morphological types for three bright galaxies in A 98 as E/SO. Owen & White (1991) discussed the R surface photometry and estimated the absolute magnitudes and the photometric structure parameters for a sample of brightest cluster galaxies and among them of 0043+2011A. We have transformed their values calculated for H_o = 75[km (s Mpc)$^{-1}$] and q_o = 0.0 and z(4C+20.04A)=0.1043 to our ones corresponding to H_o = 50[km (s Mpc)$^{-1}$] and q_o = 0.5 and z=0.1034. We calculated the absolute magnitude within the R-surface isophote of 24.5 $mag\,(arcsec)^{-2}$: M = –22.52 mag. Owen & Laing (1989) fitted the de Vacouleurs $r^{\frac{1}{4}}$ law and the power law to the surface brightness profiles using r equal to $\sqrt{(a\,b)}$

instead of a as an independent variable, where a and b are a major and a minor axis respectively. It is an important point due to the significant changes of the ellipticity, $\varepsilon = (1 - \frac{b}{a})$, with radius for many discussed galaxies. Owen and Laing estimated the position optical angle for the surface isophote of 24.5 $mag\,(arcsec)^{-2}$, $PA_{\rm opt}$= 165 deg and its ellipticity equal to 0.46. Hence, 0043+2011A has the following physical parameters: r_e = 13.94 arcsec (35.378 kpc), which we assume as the scale of the pressure gradient within the ISM and r[24.5] = 27.99 arcsec (71.033 kpc). Therefore, using the definition of r and the value of ε we derived the equivalent axes and axes for the surface brightness isophote of 24.5 $mag\,(arcsec)^{-2}$, as follows: a_e = 18.97 arcsec (48.143 kpc), b_e = 10.24 arcsec (25.997 kpc), a[24.5] = 38.09 arcsec (96.664 kpc) and b[24.5] = 20.57 arcsec (52.199 kpc), where a[24.5] and b[24.5] refer to the surface isophote of 24.5 $mag\,(arcsec)^{-2}$.

The radio galaxy 4C+20.04A has been observed at different radio wavelengths by different authors. Its mean spectral index between 6 and 20 cm is SP=0.87 ($S_\nu \sim \nu^{-SP}$). Lets us only mention the discussions by O'Donoghue et al. (1990, 1993) at 1452 MHz, Owen et al. (1992) , Giovannini et al. (1987) and Feretti et al. (1990). In the discussion we have used the VLA radio data at 20 cm published by O'Donoghue et al. (1990) after the transformation to the assumed cosmological model, i.e. H_0 = 50[km (s Mpc)$^{-1}$] and q_0 = 0.5. The WATs usually have a weak radio core and extended jets and lobes. Their jets are often bent by ram pressure. Generally, the strongest bending occurs at the hot spots. After that the tails can show some bending but they usually stay straight at the larger distances from the core. O'Donoghue et al. (1990) have given among others the changes of physical parameters of the S and N jets of 4C+20.04A with the distance from the core derived from the VLA observations at 1452 MHz. The two jets differ in their radio fluxes as well as in the diameter and the internal pressure changes.

We compared the minimum pressures P_{min} in the jets with the thermal pressure distributions calculated in previous Section (Fig.5). It is seen in Fig.5 that P_g become higher than P_{min} in the S jet at a distance of about 40-50 arcsec, which corresponds approximately to the edge of the major axis of the isophote of 24.5 $mag\,(arcmin)^{-2}$ (the ISM/ICM interface). At this distance, the jet emerges from the protecting ISM and encounters the moving IGM/ICM. It becomes unstable due to the IGM/ICM flow and is disturbed. The slight shock may form at this point.

Jets of WATs are often interpreted as subsonic steady-state flows collimated and confined by the thermal pressure of the external gas. However, this is not always true and then other steady-state models of freely expanding jets and magnetically confined jets have been proposed, although these models also have problems. Besides, one has to be aware that the estimations of thermal and non-thermal pressures are very uncertain. Firstly, the absolute position from the Einstein IPC has a 90 % confidence uncertainty of about 30 arcsec. Secondly, the low resolution of the IPC do not allow us to recognize the small scale, high density regions. Accordingly, the actual pressure of gas surrounding radio features may be much greater than the large scale average, that we calculated. Therefore, if small scale

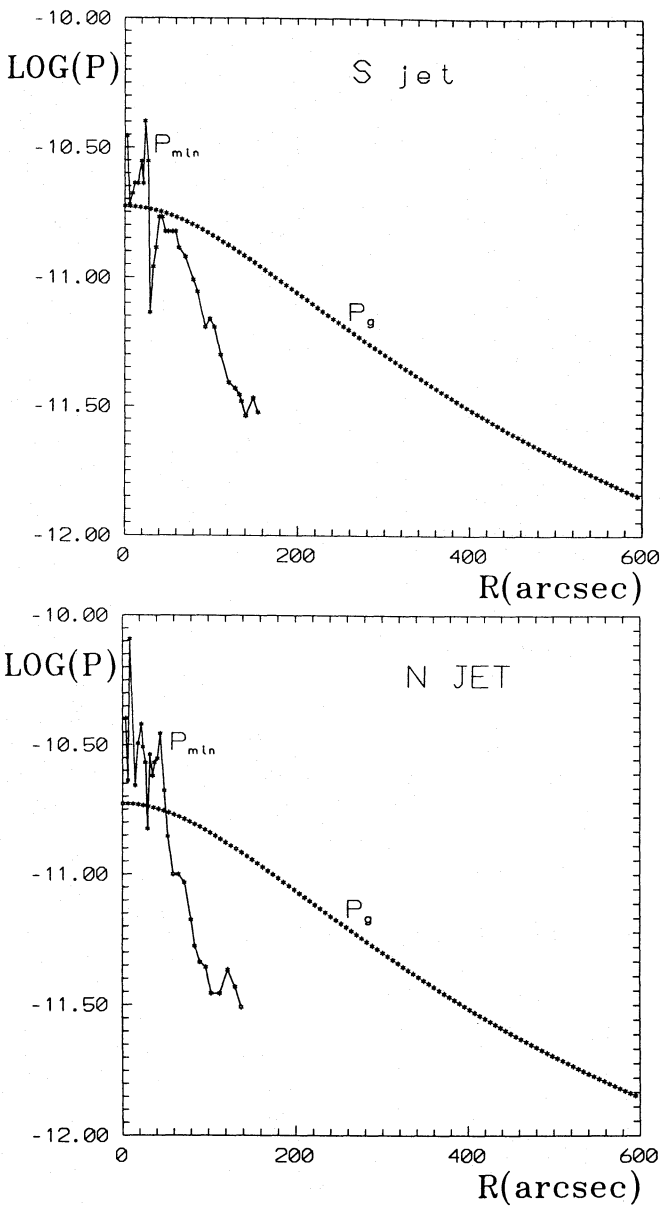

Fig. 5. Comparison of the thermal pressure distribution P_g in A 98S with the nonthermal one P_{min} in the jets of 4C+20.04A

gas feature of high density are present, the ratio of P_{th}/P_{min} could be underestimated close to the core. Finally, we are aware of projection effects. Hence, the low ratios of P_{th}/P_{min} in regions close to the radio core are not necessarily indicative of a pressure imbalance, since the dimensions of jets close to the core are not well determined. On the other hand, such an overpressure of P_{min} may be real, since it may be impossible to confine statically the first part of a jet. Nevertheless, according to a criterion proposed by Morganti et al. (1988) the external and the internal gas is really out of equilibrium if the pressure ratios are greater than 3 up to 6, what is not satisfied for the jets in 4C+20.04A.

There is a low luminosity gap in the region near the nucleus of 4C+20.04A, which confirms the F-R II - F-R I conversion

process (De Young 1993). On the other hand, basing upon the VLBI observations of a few radio galaxies of the F-R I type Giovannini et al. (1994) have not found any difference between their radio morphologies and those of the F-R II ones at parsec scale. Hence, the large morphological difference between these two types of radio galaxies on the kpc scale is due to the differences in the surrounding medium on these scales.

At 20 cm both jets in 4C+20.04A are unresolved up to distances of about 27.1 and 27.6 arcsec for the northern and the southern ones respectively. Then, they broaden, flare and terminate in hot spots. The northern hot spot (40 % polarized) is smaller and more pronounced at a distance of about 37 arcsec, while the southern one (between 20 % and 30 % polarized) is more extended at about the same distance. The position angle of radio structure of 4C+20.04A is consistent with the optical one and with the positional angle of A 98N center in A 98. Assuming that the jets are intrinsically symmetric, we constrained the value of $\beta \cos\theta$ from the sidedness ratio S, according to the formula:

$$S = (1 + \beta \cos\theta)^{2+SP} (1 + \beta \cos\theta)^{-(2+SP)}$$

where β is the ratio of the jet velocity to the light velocity ($\beta = \frac{V}{c}$) and θ is the angle between jet direction and the line of sight. For the mean spectral index SP equal to 0.87 and S=1.5 the derived constraints are drawn in Fig.6. It is seen in Fig.6 that 4C+20.04A lies almost on the plane of sky with $\beta \geq 0.2$ and $\theta \geq 69deg$. The increase of SP will give the larger inclination angles.

We consider the hot spots as the places where the jets bend, broaden (disrupt) and merge into tails. The observed almost straight radio structure of 4C+20.04A is just due to the motion of the galaxy in respect to subcluster A 98S parallel to the line of sight, what seems to be supported by dynamical considerations. The additional bending and distortions of radio tails, particularly of the northern one may be due to the merger of subclusters. 0043+2011A moves with the radial velocity of about -490, -319 and -83 [km s^{-1}] in respect to A 98S, A 98 and A 98N respectively.

Instabilities and disruptions of jets are described in a variety of numerical hydrodynamic and/or magnetohydrodynamic simulations of jets (e.g. Hardee et al. 1991; Zhao et al. 1992). Zhao et al. (1992) have discussed the disruption of the extragalactic jets, in WATs among others, due to small disturbances. Such disturbances may excite the instabilities within the jets characterized by growing internal body waves and the coupled surface waves. These waves eventually disrupt the jet at a certain lenght, namely the disruption length (l_{dspt}). Zhao et al. (1992) have given the relation between l_{dspt}, the jet internal Mach numbers (M_{in}) and the perturbation intensity ($\frac{\rho'}{\rho_o}$). In WATs the initial perturbation can be excited by the motion of the parent galaxy through the ICM, by the merger of subclusters and by shock at the ISM/ICM interface. We have used above mentioned relations to estimate the jet internal Mach numbers for 4C+20.04A. Having the VLA observations by O'Donoghue et al. (1990) we can determine the average jet pressure (P^{av}_{min}),

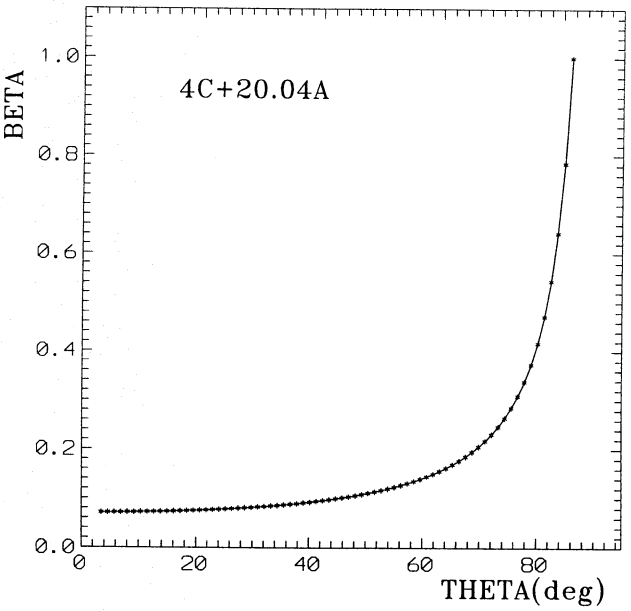

Fig. 6. Constraints on θ, the angle between the jet and the line of sight, and β, the jet velocity relative to the light velocity, derived from jet/counterjet ratio. The allowed values are on the right of the curve

its standard deviation (σ_P) and l_{dspt}. Then, the initial density perturbations are given by:

$$\left(\frac{\rho'}{\rho_o}\right) = f^{-1}\,\Gamma^{-1}\left(\frac{\sigma_P}{P^{av}_{min}}\right). \quad (1)$$

Assuming for the adiabatic index $\Gamma = \frac{5}{3}$ and for the growth factor of the jet density in WATs, f = 10, we derived the initial perturbation intensity ($\frac{\rho'}{\rho_o}$) equal to about 0.03 (3 %) and 0.02 (2 %) for N and S jets respectively. For measured l_{dspt}, namely about 19 R and 17 R (where R is the half width of the slab jet, i.e. 2.33 (N) and 3.82 arcsec (S jet)) for the N and S jets respectively, we estimated M_{in} smaller than 3. The projection effect, i.e. the inclination of the jets to the plane of sky, results in an underestimation of l_{dspt} and consequently of M_{in}.

Accordingly, assuming that the straigthness of jets of 4C+20.04A is due to the projection and that the small initial perturbations of the order of a few percent (2 % or 3 % as discussed above) might disrupt jets we consider the bending of tails of radio galaxy. The rate of bending of the jets is governed by the jet density profiles and one needs to know the flow velocity at the bend. It is common to use the surface brightness of the jet/tail to constrain the flow field. Two simple models, namely the adiabatic and the kinetic ones, have usually been considered to relate the surface brightness and dynamics of tailed radio sources. We limited our discussion to the adiabatic one, in which the relativistic particles are initialy energized in a core and lose their energy without the reacceleration as they flow along jets or tails. Besides, a steepening of the observed synchrotron power spectrum occurs due to radiative losses during moving down the tail. However, only the fraction of the net energy flux carried by the relativistic particles, so called adiabatic

efficiency - ϵ_{ad}, contributes to the synchrotron radiation. We treat ϵ_{ad} as constant, although it should change with the position in the tail and with the age of the source. To derive the flow velocity at the bend in each tail, we use the approach of Owen et al. (1985). Hence, for a power-law electron distribution, i.e. $N(E) = N_o\, E^{-\gamma}$, the synchrotron volume emissivity is given by $j_\nu = c_5(\gamma) \cdot N_o (B \sin\vartheta)^{0.5(\gamma-1)} (\frac{\nu}{2\,c_1})^{0.5(1-\gamma)}$. Here γ is the electron energy spectral index, which relates to the spectral index SP by $\gamma = 2\,SP + 1$, ϑ - the angle between the magnetic field B and the line of sight and c_1, c_5 are constants given by Pacholczyk (1970). Since the magnetic flux and the number of relativistic particles are conserved in the beam in discussed model, the evolution of dominantly parallel B^{pl} and perpendicular magnetic field B^{pr} differ, i.e. $B^{pl} \propto R^{-2}$, $B^{pr} \propto (RV)^{-1}$ and $N_o \propto (R^2\,V)^{-\frac{1}{3}(\gamma+2)}$., where R is the radius and V the velocity of the jet/tail. Hence, for a circular flow the luminosity of the beam per unit length is given by $L_\nu \propto j_\nu\, R^2$. After some calculations we have derived the normalized jet velocity V_j as a function of distance from the core r for the adiabatic jet model with the magnetic field parallel V_j^{pl} and perpendicular V_j^{pr} to the beam flow, as follows:

$$\frac{V_j^{pl}(r)}{\beta_o} = c \cdot \left[\frac{L(r)}{L_o}\right]^{\left(-\frac{3}{2\,SP(r)+3}\right)} \cdot \left[\frac{R}{R_o}\right]^{\left(-\frac{2\cdot(5\,SP(r)+3)}{(2\,SP(r)+3)}\right)} \qquad (2)$$

$$\frac{V_j^{pr}(r)}{\beta_o} = c \cdot \left[\frac{L(r)}{L_o}\right]^{\left(-\frac{3}{5\,SP(r)+6}\right)} \cdot \left[\frac{R}{R_o}\right]^{\left(-\frac{(7\,SP(r)+3)}{(5\,SP(r)+6)}\right)}; \qquad (3)$$

(where $\beta_o = \frac{V_o}{c}$, V_o is the initial jet velocity, R - the radius of the beam, L - the jet radio luminosity derived for the adiabatic efficiency (ϵ_{ad}) of the order of 0.01, SP - the spectral index between 20 and 6 cm). Since the jets are only partialy resolved, i.e. about 20 % of jets are unresolved, we used half of the beamwidth as an upper limit to the radius. For L_o and R_o we have taken the mean values of L and R for the unresolved parts of jets and β_o we have considered as the free parameter. The changes of the jet velocities with the distances from the core are shown in Fig.7.

The bending points are indicated as arrows in this figure. It is known that the F-R I radio galaxies tend to have jet magnetic fields being either everywhere perpendicular to the jet or changing from the parallel on the jet edges into the perpendicular ones towards the jets axis (so called helical or tangled fields). Hence, in the considerations of bending we will use the jet velocities derived for the perpendicular component of magnetic field just to put the limits on the jet densities.

Knowing the gaseous environment of radio galaxy and its velocity relative to the cluster centroid and relative velocity of the subclusters we are able to determine the physical parameters needed to bend the jet/tail plasma flow within the context of the continuous beam model. Generally, the physics of the radio tails can be described by a nonrelativistic, hydrodynamical flow, which follows Euler equation:

$$\frac{\partial \boldsymbol{V}}{\partial t} + (\boldsymbol{V} \cdot \nabla)\,\boldsymbol{V} = \frac{\nabla P}{\rho_t} + \boldsymbol{g}. \qquad (4)$$

Here, V is the velocity, P - the pressure, ρ_t - the tail/jet density, g - the gravitational acceleration and t - the time. For assumed

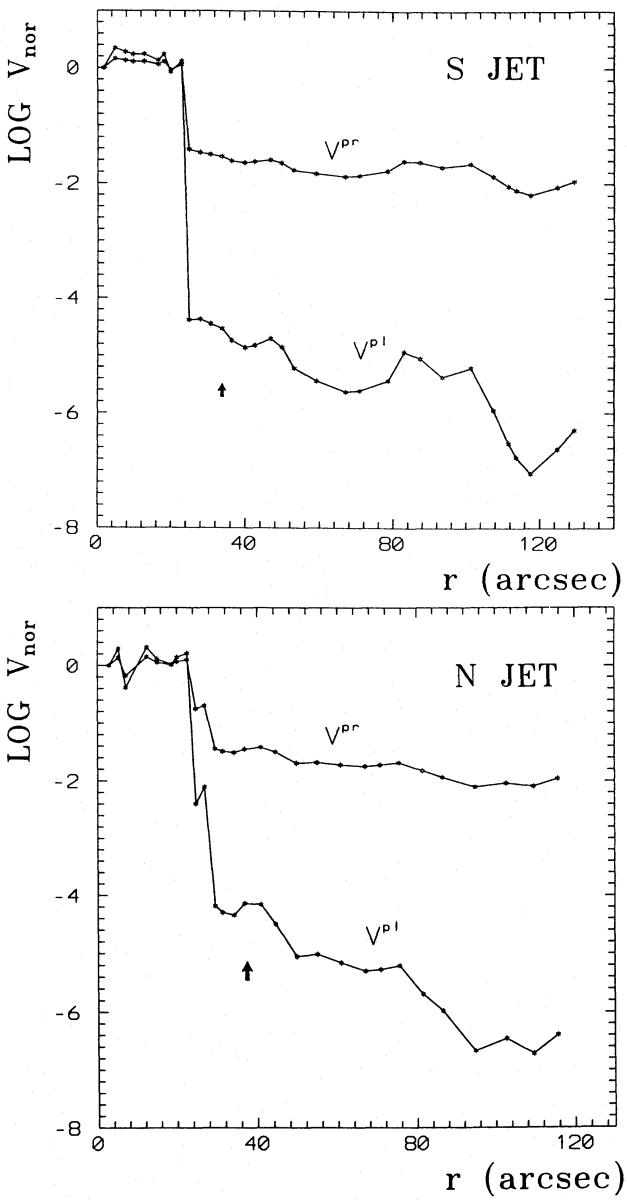

Fig. 7. Velocity curves derived from the radio luminosities for the adiabatic jet model assuming perpendicular V^{pr} (dashed lines) and parallel V^{pl} (solid lines) magnetic fields. The arrows indicate the bending points

steady flow, we put $\frac{\partial V}{\partial t} = 0$. We also neglect the gravitational acceleration g of the cluster. Then, the pressure gradient consists of the buoyancy pressure gradient in a cluster gas and of the dynamic pressure gradients arising from the slow galaxy motion with $V_g = 490[\mathrm{km\,s^{-1}}]$ in respect to A 98S and from the merger of subclusters with the relative velocity of 455 [$\mathrm{km\,s^{-1}}$]. Therefore, we have:

$$\nabla P = -kT_{gas}\frac{\partial n}{\partial r} - m_p V_g^2 \frac{n}{r_t} - m_p V_{rel}^2 \frac{n}{a_c}; \qquad (5)$$

(where n is the number gas density given in the previus Section, a_c - the X–ray core radius and r_t – the scale height of the pressure

gradient due to galaxy motion). The first term in the pressure gradient is the radially directed buoyancy pressure gradient, the second and the third ones are the dynamic pressure gradients due to the galaxy motion and the merger of subclusters respectively. After some calculations, the Euler equation has a form:

$$V_j^2 \cdot \frac{\rho_j}{l_{bend}} = 3\beta_{spec} n_o \cdot \frac{r}{a_c^2} \cdot \left[1 + (\frac{r}{a_c})^2\right]^{-\left(\frac{3\beta_{spec}}{2}+1\right)}$$
$$+ (m_p\, n_o) \cdot \left[1 + (\frac{r}{a_c})^2\right]^{-\left(\frac{3\beta_{spec}}{2}\right)} \left(\frac{V_g^2}{r_t} + \frac{V_{rel}^2}{a_c}\right);$$

(where V_j is the jet velocity as above mentioned, ρ_j – the jet density and l_{bend} – the bending scale). We have assumed for r_t the values of the equivalent radius of the parent galaxy, i.e. 13.94 arcsec (35.378 kpc) for the distances from the core smaller than 27.99 arcsec and for larger distances the values of the beam radius at the bending points, i.e. 2.63 (6.741 kpc) and 3.82 arcsec (9.794 kpc) for the N and S jets respectively. Putting the latter values of r_t we assumed the unshielded beam and obtained the strongest bending. Hence we have used in the calculations: β_{spec} = 0.76, kT = 7 keV, a_c = 3.40 arcmin (526 kpc), n_o = $1.67 \cdot 10^{-3}$ cm^{-3}, l_{bend} = 13.57 arcsec (34.841 kpc) for N tail, and 29.78 arcsec (76.384 kpc) for S tail. We derived the values of all the pressure gradients to compare them with the jet pressures at the bending distances, for which we put the approximate distances of hot spots, namely 33.8 and 36.9 arcsec for the S and N tails respectively. For the above mentioned parameters, they are, as follows:

- the buoyancy pressure gradient – $4.1 \cdot 10^{-33}$ (S) and $4.4 \cdot 10^{-33}$[dyn cm^{-2} cm^{-1}] (N tail);
- the ram pressure due to galaxy motion – $2.1 \cdot 10^{-31}$ (S) and $3.1 \cdot 10^{-31}$[dyn cm^{-2} cm^{-1}] (N tail);
- the ram pressure due to the merger of subclusters – $3.4 \cdot 10^{-33}$[dyn cm^{-2} cm^{-1}] for both tails.

Hence the whole pressure gradients are of the order of $3.2 \cdot 10^{-31}$ and $2.2 \cdot 10^{-31}$[dyn cm^{-2} cm^{-1}] for N and S tails respectively. The increase of central density n_o and the decrease of the X–ray radius a_c will lead to the rise of pressure gradients. On the other hand, if we will use the tail radii instead of the X – ray core radius in the calculations of the ram pressure due to merger of subclusters we will obtain the ram pressures of the order of $5.2 \cdot 10^{-30}$ and $3.6 \cdot 10^{-30}$[dyn cm^{-2} cm^{-1}] for N and S tails respectively.

However, one can describe the bending only if the mean density ρ_j and the mean velocity V_j of the jet/tail, in the region where the flow bends, are evaluated. Since the bending points in 4C+20.04A are not well determined, we have taken quite a wide region for the bending scales and calculated the average values of the above mentioned quantities. The average velocities are derived relative to β_o.

We calculated the left side of the Euler equation by two different ways. In the first method we took the estimated jet velocities and the above quoted values of l_{bend} to derive the upper limits upon the jet densities, which may be bent. Then, we compared these densities ρ_j with those derived from P_{min}. In the second method we assumed $\rho_j = 0.1 \cdot \rho_g$ (e.g., Morganti et al. 1987) and for the calculated jet velocities and l_{bend} we estimated the values of the left sides of the Euler equations to compare them with those of the right ones. Besides, in both methods we considered the values of the above quoted quantities at the bending points and their mean values within the bending scale. Such estimated jet densities agree within the factor of 1.1. Since we calculated the jet velocity relative to $\beta_o = \frac{V_o}{c}$, which is not exactly known, the estimated jet densities for $\beta \geq 0.2$ (see Fig. 6) and for the perpendicular magnetic field are:

- for N jet – $\rho_j \leq 6.5 \cdot 10^{-28}$ and $\leq 2.0 \cdot 10^{-27}$g cm^{-3} as derived from P_{min} and the total ram pressure respectively,
- for S jet – $\rho_j \leq 7.6 \cdot 10^{-28}$ and $\leq 5.9 \cdot 10^{-27}$g cm^{-3} as quoted above.

Accordingly, the comparison of these two values of jet densities indicates that the bending of jets in 4C+20.04A may result from the buoyancy pressure gradient and from ram pressure due to galaxy motion and the merger of subclusters.

However, it is known that the adiabatic models are the simplest ones and are in trouble with travel times much longer than the particle lifetime. In real relativistic flows the different kinds of particle acceleration in - situ are needed (Achtenberg 1987). The inhomogeneous jet model with the velocity structure across the jets at all distances from the core and the deceleration of outer layers of jets due to their interactions with the surrounding seems to be more realistic. Unfortunately, such model contains many free parameters, so is hard to test quantitatively.

4C+20.04B (z=0.1044, $\frac{r}{A_R}$(A 98)=0.62) is a weak radio galaxy, with an extended radio structure laying at a distance of 4.48 $arcsec$ from center of A 98N, where $P_g = P_{th} = 4.2\,10^{-12}$[dyn cm^{-2}]. Its light–of–sight velocities are 172 and -71[km s^{-1}] relative to A 98N and A 98 respectively.

Summarizing, if the straightness of jets in the WAT radio galaxy, 4C+20.04A, is due to the projection effects, the bending of tails may result from the ram pressure caused by the motion of galaxy, by merger of subclusters and by buoyancy pressure gradient. On the other hand, the merger of subclusters will distort the X – ray brightness isophotes in the beginning along the collision axis and later perpendicular to it. There are some indications that such a distortion appears approximately along the (A 98S-A 98N) direction (Feretti et al. 1990). The X-ray observations of higher spatial resolution (e.g. ROSAT HRI) are desirable to confirm them.

Acknowledgements. We would like to thank the referee for his valuable comments. This work was partly supported by a Nicolaus Copernicus University grant No 685-A.

References

Achtenberg et al., 1987, in: Astrophysical Jets and Their Engines, ed. W. Kundt, Dordrecht - Holland, D.Reidel Publ. Co., pp.211-222
Abell G. O., Corwin, H. G., Olowin, R. P., 1989, ApJS 70, 1
Bahcall N. A., Cen R., 1993, ApJ 407, L49
Bahcall N. A., Lubin L.M., 1994, ApJ, in press
Ball R., Burns J. O., Loken Ch., 1993, AJ 105, 53
Beers T. C., Flynn K., Gebhardt K., 1990, AJ 100, 32
Beers T. C., Geller M. J., Huchra J. P., 1982, ApJ 257, 23
Beers T. C. et al., 1991, ApJ 257, 23

Bergmann A. G., Petrosian V., Lynds R., 1990, ApJ 350, 23
Blandford R. D., Kochanek C. S., 1987, ApJ 321, 658
Briel U. G. et al., 1992, A&A 259, L31
Burns J. O., 1990, AJ 99, 14
Burns J. O. et al., 1994, in: Proceeding of the ROSAT Science Symposium, ed. E. M. Schlegel & R. Petre, NY: AIP, in press, NRAO – 94/5
Cavaliere A., Fusco-Femiano R., 1981, A&A 233, 325
Danese L., De Zotti G., di Tullio G., 1980, A&A 82, 322
Davis D. S., Mushotzky R. F., 1993, AJ 105, 409
De Young D. S., 1993, ApJ 405, L13
Dressler R., 1978a, ApJ 223, 765
Dressler R., 1978b, ApJ 226, 55
Edge A. C., Stewart G. C., 1991, MNRAS 252, 428
Faber S. M., Dressler A., 1977, AJ 82, 187
Feretti L., et al., 1990, A&A 233, 325
Fitchett M., Webster R., 1987, ApJ 317, 653
Forman W., Jones C., 1982, ARA&A 20, 547
Forman W. et al., 1981, ApJ 243, L137
Giovannini G. et al., 1987, A&AS 69, 171
Giovannini G. et al., 1994, in: Compact Extragalactic Radio Sources, Proceedings of the NRAO Workshop No. 23, ed. J. A. Zensus & K. I. Kellermann, Green Bank, pp.61 - 66
Hardee P. E., Norman M. L., Koupelis T., Clarke D. A., 1991, ApJ
Henriksen M. J., 1993, ApJ 407, L13
Henry J. P., Henriksen M. J., Charles P. A., Thorstensen M. J., 1981, ApJ 317, 653
Henry J. P., Briel U. G., Nulsen P. E., 1993, A&A 271, 413
Lubin L. M., Bahcall N. A., 1993, ApJ 415, L17
Malumuth J., 1992, ApJ 386, 420
Mc Glynn T. A., Fabian A. C., 1984, MNRAS 208, 709
Mollier Y., Fort B., Kneib J–P., 1993, ApJ 407, 33
Morganti R. et al., 1987, A&A 183, 203
Morganti R. et al., 1988, A&A 189, 11
O'Donoghue A., Eilek J. A., Owen F. N., 1993, ApJ 408, 428
O'Donoghue A., Owen F. N., Eilek J. A., 1990, ApJS 72, 75
Owen F. N., Laing R. A., 1989, MNRAS 238, 357
Owen F. N., O'Dea C. P., Inoue M., Eilek J. A., 1985, ApJ 294, L85
Owen F. N., White R. A., 1991, MNRAS 249, 164
Owen F. N., White R. A., Burns J. O., 1992, ApJS 80, 501
Pacholczyk A. G., 1970, Radio Astrophysics, Freeman, San Francisco
Peebles P. J. E., 1992, Principles of Physical Cosmology, Princeton University Press, Princeton
Rhee G. F. R. N., van Haarlem M. P., Katgert P., 1991, A&A 233, 325
Roettiger K., Burns J., Loken Ch., 1993, ApJ 407, L53
Salvador-Solé E., Gonzáles-Casado G., Solanes J. M., 1993, ApJ 410, 1
Sandage A., 1973, ApJ 183, 731
Sandage A., Hardy E., 1973, ApJ 183, 743
Sarazin C. L., 1992, in: Cluster and Superclusters of Galaxies, ed. A. C. Fabian, Dordrecht:Kluwer, p. 131
Schindler S., Böhringer H., 1993, A&A 269, 83
Schindler S., Müller E., 1993, A&A 272, 137
Schneider D. P., Gunn J. E., Hoessel J. G., 1983, ApJ 268, 476
Schwarz R. A., 1992, A&A 233, L11
Slingo A., 1974, MNRAS 168, 307
Struble M. F., Rood H. J., 1987, ApJS 63, 543
Turner E. L., Ostriker J. P., Gott III J. R., 1984, ApJ 284, 1
Tyson J. A., 1988, ApJS 63, 543
Tyson J. A., Valdes F., Wenk R. A., 1990, ApJ 349, L1
White III R. E., 1991, ApJ 317, 653
Yahil A., Vidal N. V., 1977, ApJ 214, 347
Zabludoff A. I., Huchra, J. P., Geller, M. J., 1990, ApJS 74, 1
Zhao J. H., Burns J. O., Norman M. L., Sulkanen M. E., 1992, ApJ 387, 69
Zhao J. H., Burns J. O., Owen F. N., 1989, AJ 98, 64

This article was processed by the author using Springer-Verlag LaTeX A&A style file version 3.